Biomedicine & Pharmacotherapy 158 (2023) 114111

Contents lists available at ScienceDirect

Biomedicine & Pharmacotherapy

journal homepage: www.elsevier.com/locate/biopha

Proteomic alterations in the cerebellum and hippocampus in an Alzheimer's disease mouse model: Alleviating effect of palmatine

Irem Kiris [a], Wirginia Kukula-Koch [b], Merve Karayel-Basar [a], Busra Gurel [c], Julide Coskun [d], Ahmet Tarik Baykal [e,*]

[a] Department of Biochemistry and Molecular Biology, Institute of Health Sciences, Acibadem Mehmet Ali Aydinlar University, Istanbul, Turkey
[b] Department of Pharmacognosy with Medicinal Plants Garden, Medical University of Lublin, Lublin, Poland
[c] Sabanci University Nanotechnology Research and Application Center, SUNUM, Istanbul, Turkey
[d] Acibadem Labmed Clinical Laboratories, Istanbul, Turkey
[e] Department of Medical Biochemistry, Faculty of Medicine, Acibadem Mehmet Ali Aydinlar University, Istanbul, Turkey

ARTICLE INFO

Keywords:
Alzheimer's Disease
5xFAD
Palmatine
Neurodegeneration
Label-free Proteomics

ABSTRACT

Alzheimer's disease (AD) is one of the most prevalent diseases that lead to memory deficiencies, severe behavioral abnormalities, and ultimately death. The need for more appropriate treatment of AD continues, and remains a sought-after goal. Previous studies showed palmatine (PAL), an isoquinoline alkaloid, might have the potential for combating AD because of its in vitro and in vivo activities. In this study, we aimed to assess PAL's therapeutic potential and gain insights into the working mechanism on protein level in the AD mouse model brain, for the first time. To this end, PAL was administered to 12-month-old 5xFAD mice at two doses after its successful isolation from the *Siberian barberry* shrub. PAL (10 mg/kg) showed statistically significant improvement in the memory and learning phase on the Morris water maze test. The PAL's ability to pass through the blood-brain barrier was verified via Multiple Reaction Monitoring (MRM). Label-free proteomics analysis revealed PAL administration led to changes most prominently in the cerebellum, followed by the hippocampus, but none in the cortex. Most of the differentially expressed proteins in PAL compared to the 5xFAD control group (ALZ) were the opposite of those in ALZ in comparison to healthy Alzheimer's littermates (ALM) group. HS105, HS12A, and RL12 were detected as hub proteins in the cerebellum. Collectively, here we present PAL as a potential therapeutic candidate owing to its alleviating effect in 5xFAD mice on not only cognitive impairment but also proteomes in the cerebellum and hippocampus.

1. Introduction

Alzheimer's disease (AD) is one of the leading health problems characterized by memory deficiencies, severe behavioral abnormalities, and ultimately – death [1]. The pathological markers of AD, amyloid-beta (Aβ) plaques and neurofibrillary tangles (NFTs), have been the same ever since they were described by Alois Alzheimer in 1907 [2,3]. The number of AD patients is increasing each year drastically and is expected to reach 78 million in 2030, and as of 2021 AD is reported to be the 7th leading cause of death in the world [1]. Current drugs mostly provide temporary relief and slow down the progression of mild to moderate stages of the disease. Aducanumab is the first disease-modifying drug that is approved under the FDA-accelerated approval pathway but it remains questionable [4]. Therefore, it is crucial to find medications to cure, reverse or halt the progress of AD.

Nature is a library of chemical structures, and the search for suitable drug candidates often begins with the plant extracts which are their primary source. Palmatine (PAL), an isoquinoline alkaloid, is reported to have a wide range of properties such as anti-cancer, anti-bacterial, anti-viral, anti-inflammatory, blood-lipid regulating, and neuroprotective activities [5]. Also, PAL was proved to exhibit acetylcholinesterase and butyrylcholinesterase inhibitory activity [6,7]. Additionally, performed in vitro assays proved that the formation of Aβ plaques and the aggregation of tau protein were reduced in the presence of PAL [8]. In other

Abbreviations: DEP, Differentially expressed protein; AD, Alzheimer's disease; PAL, Palmatine; ALM, Alzheimer's littermate.

* Correspondence to: Acibadem Mehmet Ali Aydinlar University, Department of Medical Biochemistry, School of Medicine, Icerenkoy Mah. No: 32, Kayisdagi Cad., 34752 Ataşehir, Istanbul, Turkey.
E-mail address: ahmet.baykal@acibadem.edu.tr (A.T. Baykal).

https://doi.org/10.1016/j.biopha.2022.114111
Received 17 October 2022; Received in revised form 28 November 2022; Accepted 6 December 2022
Available online 8 December 2022

studies the alkaloid exhibited procognitive effect in scopolamine- and diazepam-induced amnesia in Swiss young male albino mice [9]. Given together, the results of previously published studies show that PAL might have a potential for combating AD owing to its proved in vitro and in vivo activities.

Mouse models are invaluable assets for examining the mechanisms of human diseases and researching therapeutical strategies. The transgenic mouse that carries 5 Familial Alzheimer's disease mutations (5xFAD), is a widely preferred model for AD studies (~10 %) because of a rapid exhibition of most of the pathologic alterations that are present in human AD, namely: Aβ-plaques, synaptic degeneration, gliosis, neuronal loss and progressive cognitive impairment [10,11]. Age-dependent memory loss begins in 5xFAD mice at the age of 6 months and progresses from this time on; likewise, the histopathological symptoms of the acquired disease progressively worsen with time [12–15]. Additionally, changes in gene expression were found to be better in recapitulating the human AD brain with increased age [10] and related pathways of 12-month-old 5xFAD mice were strikingly similar to those of human AD [16,17]. In light of the given information, 12-month-old 5xFAD mice offer a suitable model for investigating the efficacy of the potential therapeutics.

Thanks to the application of proteomic studies the molecular pathomechanisms of the disease and of the drug candidates may be revealed [18,19]. Unbiased, label-free liquid chromatography coupled to tandem mass spectrometry (LC-MS/MS) is a powerful tool that is able to take the functional snapshot of the cell, then accurately identify thousands of proteins engaged in the progression of the disease, and to provide relative quantification thereof at that moment [20,21].

This study aimed to assess PAL's therapeutic potential and to reveal its effect on protein level in the AD mouse brain regions, for the first time. To this end, after its successful isolation from the *Siberian barberry* shrub, PAL was administered to 12-month-old 5xFAD mice at two doses (5 mg/kg and 10mg/kg, i.p.) for 7 consecutive days. PAL's possible effects on cognition were evaluated by the Morris water maze (MWM) test. The blood-brain passage of the substance was verified by MRM. Also, using the nLC-MS/MS, proteomic expressional changes were analyzed in the cortex, hippocampus, and cerebellum regions, individually. As a result of bioinformatic analysis, the identification of possible key proteins engaged in the molecular mechanism of PAL were revealed, and their expressions were validated through the Western blot method.

2. Materials and methods

2.1. Reagents

Gradient grade reagents used for the extraction of the roots and isolation of PAL (methanol, ethanol, butanol, ethyl acetate) were obtained from Avantor Performance Materials (Gliwice, Poland). The HPLC-MS purity solvents (water, acetonitrile, formic acid) used in the HPLC-ESI-QTOF-MS/MS analysis were purchased from Merck (Darmstadt, Germany).

2.2. Plant material and extraction

The underground parts of *Berberis sibirica* Pall. were collected in the vicinity of Ulanbataar by Dr. Otgonbataar Urjin from the Mongolian National University of Medical Sciences, Mongolia in the summer of 2010, and they were stored in the dark at the Department of Pharmacognosy with Medicinal Plants Garden of the Medical University of Lublin, Poland by Wirginia Kukula-Koch. The extraction of the root powder was performed by accelerated solvent extraction (ASE 100, Dionex, Sunnyvale, CA, USA) in the following conditions: extracting solvent: methanol, temperature: 70 °C, pressure: 110 bar, static time: 10 min, purge time: 80 s, purge volume: 80 s, number of cycles: 5. In each instance, 25 g of the powdered plant material was transferred to a stainless-steel vessel and subjected to the extraction process. The extracts were pooled and evaporated under reduced pressure on a rotary evaporator at 50 °C. Every extraction provided approximately 16.5 % of a dried residue that was extracted from the plant matrix.

2.3. The isolation of palmatine by centrifugal partition chromatography (CPC)

The isolation of PAL was performed on a Centrifugal Partition Chromatograph (Spot-CPC-250-L) produced by Armen Instrument (Saint Ave, France) that was equipped with a 250 mL rotor, a quaternary pump, a UV detector, and a fraction collector produced by the same company. The analysis was performed as described in a former study [22] using the following biphasic solvent system: butanol: ethanol: ethyl acetate: and water (1:1:3:6 v/v/v/v) in the ascending operation mode. Briefly, the column was first filled with a stationary phase at the flow rate of 20 mL/min. Later, the mobile phase was pumped on the column together with the extract dissolved in 4 mL of a 50: 50 (v/v) mixture of upper and lower phases. The flow rate was set at 6 mL/min, the detection wavelength at 280 and 320 nm, the elution time at 30 min, and the extrusion time at 50 min. Around 200 mg of the total extract was injected in each run to provide high purity PAL. 18 mL-volumed fractions were collected through the analysis. Based on the high-performance liquid chromatography mass spectrometry (HPLC-MS) analysis, similar fractions were pooled and evaporated to dryness at 50 °C on a rotary evaporator under reduced pressure.

2.4. HPLC-ESI-QTOF-MS/MS analysis of the total extract and fractions from the CPC separation

An Agilent Technologies (Santa Clara, CA, USA) HPLC-ESI-QTOF-MS/MS composed of high-performance liquid chromatograph (1200 Series) coupled with a mass spectrometer (6500 Series) were used in the study. The previously elaborated method provided high sensitivity, good efficiency, and high mass measurement accuracy in the analysis of *Siberian barberry* extract and its fractions. The instrument was used for the determination of the composition and purity assessment. It was operated in the positive ionization mode and under the following settings: gas and sheath gas temperatures: 350 and 325 °C, respectively, gas and sheath gas flows: 12 L, capillary voltage: 3500 V, fragmentor voltage: 120 V, collision energies: 20 and 40 V, skimmer voltage: 65 V, nebulizer pressure 30 psig. The Zorbax Eclipse Plus C-18 reversed phase chromatographic column (Agilent Technologies, Santa Clara, CA, USA) was used for the separation of metabolites in the described conditions above. The following gradient of acetonitrile with 0.1 % of formic acid (A) in 0.1 % formic acid in water was applied: 0 min 10 % A, 10–12 min 40 % A, 21 min 95 % A. The flow rate was 0.2 mL/min, the run length was 30 min and the temperature of the thermostat was 25 °C. For the handling of spectra, the MassHunter Workstation program (version B.08.00) by Agilent Technologies (Santa Clara, CA, USA) was used.

2.5. Animals and natural compound administration

The 5xFAD transgenic mouse model (Tg6799, Stock #034840-JAX) carries a total of 5 familial AD mutations in APP and PSEN1 transgene, and heterozygous B6SJLF1/J mice (Stock #100012), were supplied from The Jackson Laboratory. Mice were bred by crossing these two species and genotyping was performed with polymerase chain reaction using genomic DNA taken from ear biopsies. The protocol provided by The Jackson Laboratory was followed with the designed oligonucleotide primers (listed in Supplementary File 1). The cycling conditions were as follows: 3 min at 94 °C, 35 cycles of 30 s each at 94 °C, 60 s at 57.3 °C, 60 s at 72 °C, and 2 min at 72 °C. On a 3 % agarose gel, bands were observed using Tris-acetate-EDTA running buffer containing 1X Gel Loading Dye (NEB B7021-S) after 45 min run at 80 V (Supplementary File 1). Mice were kept at 20 °C and 12 h day/12 h night cycle, food and water were available ad libitum.

PAL extracts dissolved in DMSO or DMSO (maximum 1 %) in saline solution as a vehicle control were intraperitoneally administered to 12-month-old 5xFAD mice and their age-matched non-transgenic Alzheimer's littermates (ALM) over a period of 7 consecutively. The groups were constructed as given below:

ALM (n = 6): Alzheimer's littermates – treated with DMSO (healthy vehicle control)

ALZ (n = 8): 5xFAD Alzheimer's mouse model treated with DMSO

PAL1 (n = 7): 5xFAD mice treated with 5 mg/kg PAL

PAL2 (n = 6): 5xFAD mice treated with 10 mg/kg PAL

The gender of the mice was distributed equally, with the exception of one additional male in PAL1. After the behavioral tests, following the anesthesia with isoflurane, mice were decapitated. The brains were removed within one minute and preserved at – 80 °C for further experiments either as a whole or dissected into three regions.

2.6. Morris water maze test

The mice's spatial memory was assessed by the MWM as previously described [23]. Briefly, on day 0, mice were habituated to water and the environment. The next day, mice were released into water from 4 imaginary quadrants and allowed to swim for 60 s; the escape latency was recorded when the mouse found the hidden platform, if not, the mouse was placed onto the platform by an investigator, where it waited for 20 s in each case. This procedure was continued for 6 days (acquisition phase). On the 7th day (probe phase) the hidden platform was removed, and the time spent in the target quadrant was determined. All the records and analysis of the MWM were performed by fully automated Ethovision software (Noldus Information Technology Inc., Leesburg, VA, USA).

2.7. MRM-MS analysis

2.7.1. Sample preparation

The 10 μm sections of the frozen brain (n = 4) were homogenized in 50 μl methanol and 50 μl acetonitrile (ACN) by using vortex (30 s) and ultrasonic processor (10 ×10 s on ice, VialTweeter, HielScher). 1 mL acetone was added to the tube, vortexed for 2 min and centrifuged at 3500 rpm for 5 min. The supernatant was taken to a new tube and evaporated in a speed vac (Eppendorf, vacufuge plus). Then, the residue was reconstituted with a 50 μl mobile phase (30 % ACN, 70 % ammonium acetate (AA), 0.1 % formic acid (FA)).

2.7.2. HPLC conditions

Chromatography was carried out on a C18 Hypersil GOLD aQ column (2.1 mm × 50 mm, 3 μm, Thermo) at 40 °C temperature via a gradient elution with a 0.15 mL/min flow rate. The mobile phase consisted of A (0.08 % FA and 2 mmol/L AA) and B (ACN). The percentage of mobile phase B was increased from 10 to 100 over a 6 min total run time.

2.7.3. Tandem mass spectrometry

TSQ Quantum Access Max triple quadrupole mass spectrometer (Thermo Scientific) coupled with an electrospray source was used to analyse extracted tissues. Given parameters were set at: collision energy: 30 eV, collision gas pressure: 1.2 mTorr, sheath gas: 28 arbitrary units, auxiliary gas: 10 arbitrary units, capillary temperature: 350 °C and spray voltage: 3000 V. Samples were injected via syringe infusion at a flow rate of 0.15 mL/min using a Kloehn syringe WPS-3000SL (part: 6822.002). TSQ Tune software was used for scanning the samples for 6 min in profile mode. A fixed half-peak width (FWHM) of 0.7 was used.

2.7.4. Identification of palmatine

The molecular ion of $[M]^+$ PAL in the positive mode was observed at *m/z* 352. Molecular formulas of the abundant fragment ions with 336, 337, 308, and 322 *m/z* values are $[M - CH_4]^+$, $[M - CH_3]^+$, $[M - CH_4 - CO]^+$, $[M - 2CH_3]^+$, respectively. Intensity values and retention times (RT; minute) of precursor and fragment ions obtained from pure PAL were 352.100 (RT: 1.69), 336.100 (RT: 1.70), 337.100 (RT: 1.70), 308.100 (RT: 1.69) and 322.100 (RT: 1.70), respectively. Intensity values and retention times (RT; minute) of the same precursor and fragment ions with *m/z* values were investigated in order to reveal if PAL passes through the blood-brain barrier (BBB).

2.8. Nano LC-MS/MS

Brain tissues previously sectioned into the cortex, hippocampus, and cerebellum were prepared as described before [24]. Briefly, tissues were homogenized with steel beads, then lysed in UPX (Expedeon) containing protease inhibitor cocktail (Thermo Scientific) using an ultrasonic processor (VialTweeter, HielScher), and boiled for 10 min in a thermo-shaker (Biosan) at 1000 rpm and 95 °C. After cooling for 30 min at 4 °C, the samples were centrifuged for 10 min at 14000xg, and the supernatant was collected. Maximum 100 μg protein was taken from the supernatant and well-known FASP (Filter Aided Sample Preparation kit, Expedeon) [25] steps were followed: wash (8 M urea), alkylation (50 mM iodoacetamide), buffer exchange (25 mM ammonium bicarbonate) and digestion proteins into peptides (trypsin, (enzyme-to-substrate ratio 1:100)). The peptides' final concentration were adjusted to 200 μg/mL with 0.1 % FA.

The nLC-MS/MS analysis was carried out using an ACQUITY UPLC M-Class linked to a SYNAPT Xevo G2-XS system (Waters). Peptides were introduced onto a trap column (Symmetry C18 5 m, 180 m i.d. x 20 mm) initially, and then separated by gradient elution through an analytic column (CSH C18, 1.7 m, 75 m i.d. x 250 mm). As a lock mass reference, 100 fmol/μl Glu-1-fibrinopeptide B was used. Positive ion mode was used to run the device. For MS data collection, a novel data independent mode of acquisition named SONAR [26] was adopted, with a 24 Da quadrupole transmission width. Without any precursor ion preselection insensitivity mode, all ions in the 50–1950 *m/z* range were fragmented collectively [24].

For the data analysis, Progenesis-QI for proteomics software (V.2.0 Waters) and reviewed *Mus musculus* from Uniprot (database date: 13.01.2021) were used. Peak intensity thresholds were set at 60 and 10 counts for low and elevated energy, respectively. Mass data were analyzed with the following settings: the minimum number of fragmented ion matches per peptide = 2, the minimum number of fragment ion matches per protein = 5, the minimum number of unique peptides per protein = 1, and the maximum number of missed cleavage for tryptic digestion = 1, fixed modification = carbamidomethyl C, variable modifications = oxidation M and deamidation N and Q, false discovery rate (FDR) ≤ 1 %. 1 + charged ions were eliminated. Normalization between samples was performed using the total ion intensity. The statistical program contained in Progenesis QI for proteomics was used to calculate expressional changes, *p*, and *q* values. Proteins were accepted as differentially expressed if only met these criteria: ANOVA $p < .05$, $q < .05$, unique peptide > 2 and fold change ≥ 1.3.

2.9. Western blot analysis

To confirm the proteomics findings, analysis was performed with the same protein extracts that previously used for nLC-MS/MS analysis. All experiments were performed with 3 technical replicates. Lysates were mixed with 2x Laemmli sample buffer (Bio-rad) and B-Mercaptoethanol and boiled at 95 °C for 5 min. Then, an equal concentration of proteins and an unstained protein marker (Bio-rad) were loaded into a gel that was prepared as described in the TGX Stain-Free FastCast Acrylamide kit (12 %). Proteins were transferred to a PVDF membrane with Trans-Blot

Turbo Transfer System (Bio-Rad) and then blocked for 1 h in RT with 5 % skim milk (Sigma) in PBST (1 % Tween (Sigma)). Primary antibody incubations were performed overnight at + 4 °C with the following antibodies: HS105 (Santa Cruz, sc-74550, 1:100), RL12 (Biorbyt, orb315691, 1:500), HS12A (Biorbyt, orb184235, 1:500). After 3 washes with PBST, the membrane was incubated for 1 h in RT with secondary antibodies, either goat anti-mouse IgG-HRP (Santa Cruz, sc-2005, 1:4000) or goat anti-rabbit IgG-HRP (Santa Cruz, sc-6721, 1:4000). 5 min streptactin HRP conjugate (Bio-Rad, 1:10000) incubation at RT enabled visualization of the unstained marker. After washing, the image was detected using Clarity Western ECL Substrate (Bio-Rad) and ChemiDoc MP Imaging System (Bio-Rad). Image Laboratory Software Version 6.1 (Bio-Rad) was used to quantification of the bands with total protein normalization.

2.10. Statistical analysis

Statistical analysis of MWM was conducted with SPSS (version 23.0, IBM, Armonk, NY). The Shapiro-Wilks test indicated the non-normal distribution of the learning and memory phase, while the swim speeds of mice were distributed normally. For non-parametric data, statistical significance ($p < .05$) was assessed between each day of a group compared to its first day with Friedman, following its post-hoc Wilcoxon, and between the groups on a daily basis with Kruskal Wallis and its post-hoc Mann Whitney U test. Ties were corrected by using the Exact test. For normally distributed data, one-way ANOVA and its post-hoc Tukey's multiple comparisons test.

Graphpad Prism software (version 7.04 for Windows, GraphPad Software, La Jolla California USA, www.graphpad.com) was used for statistical analysis of Western blot results. Normally distributed data were assessed by one-way ANOVA (for HS105 and RL12) while Kruskal-Wallis was used for non-normally distributed data (for HS12A). If those tests showed significance, their post-hocs, unpaired t-test, or Mann-Whitney U test, respectively, were carried out. Figures of MWM and Western blots were prepared with Graphpad Prism.

2.11. Bioinformatic analysis

For Principal Component Analysis (PCA) and Hierarchical Clustering (HC), online Clustvis software was used [27]. For PCA unit variance scaling is applied to rows, and singular value decomposition (SVD) with imputation was used to calculate principal components. Prediction ellipses are such that with a probability of 0.95, a new observation from the same group will fall inside the ellipse (n = 9). Heatmap was constructed by given parameters: rows are centered; unit variance scaling is applied to rows. Rows and columns were clustered by correlation distance and average linkage. Cluster groups were constructed automatically by the software.

Gene Ontology (GO) functional enrichment analysis and Kyoto Encyclopedia of Genes and Genomes (KEGG) pathway analysis were performed in DAVID bioinformatics resources (version 6.8) [28,29] and visualized by Graphpad Prism (version 9.2.0) and Inkscape (version 1.01).

Cytoscape software (3.8.2) [30] was employed for visualizing and constructing the protein-protein interaction map and detecting hub proteins through STRING [31] database protein query, CytoNCA [32], and CytoHubba plug-ins [33] respectively. The top 3 hub proteins were revealed with CytoNCA using the Local Average Connectivity-Based Method (LAC) and CytoHubba using the Density of Maximum Neighborhood Component (DMNC) method.

3. Results

3.1. Isolation of palmatine from Berberis sibirica root methanolic extract

PAL, as a compound eluted next to berberine due to a large structural similarity in their chemical structure, was difficult to isolate using classical isolation techniques, especially those based on the use of silica gel as the stationary phase (Table 1). The conditions elaborated on with the help of a centrifugal partition chromatograph provided a clear separation of PAL from berberine and its recovery in sufficiently high quantity suitable for in vivo studies (Fig. 1). The compound was eluted from the rotating column of the CPC chromatograph within 50 min, which confirms a high selectivity of the applied solvent system composed of ethyl acetate, butanol, ethanol, and water (3:1:1:6 v/v/v/v). The purity of the isolated alkaloid was indicated by the MassHunter Workstation program and was equal to 95.77 %.

3.2. Morris water maze test

In order to reveal the effect of PAL, the cognitive differences of the 12-month-old 5xFAD mice model were evaluated with the MWM test following the compound administration. Within-group comparisons showed that the 4th day of the ALM, 4th and 5th day of the ALZ, 5th day of the PAL1, and 6th day of the PAL2 in the learning phase were significantly decreased compared to the 1st day of each group (data not shown). In the learning phase between-group comparisons reached statistical significance 4th ($X^2(3) = 12.621$, $p = .006$) and 6th ($X^2(3) = 17.177$ $p = .001$) days. Pairwise comparisons revealed that ALM, in the 4th ($U < 0$, $p = .002$) and 6th ($U < 0$, $p = .001$) day, and PAL2, in 6th ($U < 0$, $p = .001$) day in the learning phase significantly better than 5xFAD mice at finding the hidden platform (Fig. 2A). Statistical significance was reached across the groups in the probe phase ($X^2(3) = 9.496$, $p = .023$), post-hoc revealed both ALM ($U = 2$, $p = .004$) and PAL2 ($U = 8.5$, $p = .044$) spent more time in the target quadrant compared to ALZ (Fig. 2B). Analysis of variance showed swim speed varied across groups ($F(2, 15) = 11.63$, $p = .0009$). Pairwise analyses revealed that swim speed was lower for ALZ ($p = .0006$) and PAL2 ($p = .034$) in comparison to ALM. However, no statistical improvement in swim speed was detected in ALZ mice after the PAL administration ($p = .145$). These results suggest that 10 mg/kg PAL administration has a significant improving effect on learning and memory, eliminating its possible effect on motor function in ALZ. Based on these observations the same dose was selected for further analyses performed in the study.

3.3. Detection of the BBB passag of the PAL via MRM-MS

Before the investigation of the molecular alterations likely caused by PAL2, it was important to verify the BBB passage of the compound. To achieve this, PAL's precursor ion and 4 characteristic MRM fragments were scanned in the brain tissues. Pure PAL was used as a standard, precursor, and fragments were detected with the highest intensity (Fig. 3A). No precursor or fragment peak of PAL was detected in the tissue of the ALZ control group which was injected with pure DMSO into 5xFAD mouse brain (Fig. 3B). However, the precursor and all its' fragments were detected with high intensity in the PAL2 mouse brain tissue (Fig. 3C). According to the measurement of PAL in brain tissues of the PAL2 group, the BBB passage capacity of PAL were detected successfully.

3.4. Proteome analysis of the brain regions

In order to find out whether any protein expression was altered by PAL2 which improves learning and memory, the bottom-up proteomics method was used. Expressional changes in the mice brain proteome were investigated in 3 regions: cortex, hippocampus, and cerebellum. The number of identified proteins, with an estimated FDR of 1 %, across the sample set was 1704 in the cortex, 1656 in the hippocampus, and 1478 in the cerebellum (Table 2). The 7 days injection of 10 mg/kg PAL led to differential expressions (unique peptide > 2; fold change ≥ 1.3; $q < 0.05$ and $p < .05$) of 0, 8 and 110 proteins in comparison to ALZ, in the cortex, hippocampus, and cerebellum, respectively (Table 2). All

Table 1
The tentative identification of the major alkaloids in the tested methanolic extract from *Berberis sibirica* root (RDB – double bond equivalent, delta – the error of *m/z* measurement, Rt – retention time).

No	*Ionization*	*Rt (min)*	*Molecular formula*	*m/z calculated*	*m/z experimental*	*Delta (mmu)*	*RDB*	*MS/MS fragments*	*Proposed compound*	*References*
1	$[M+H]^+$	5.86	$C_{18}H_{21}NO_3$	300.1594	300.1618	-7.96	9	255, 161	N-Methylcoclaurine	[34]
2	$[M+H]^+$	6.14	$C_{19}H_{23}NO_3$	314.1751	314.1776	-8.08	9	299, 269, 237	Armepavine	[35]
3	$[M+H]^+$	8.1	$C_{20}H_{24}NO_4$	342.1700	342.1724	-7.08	10	297, 282, 265	Magnoflorine	[36]
4	$[M+H]^+$	9.44	$C_{19}H_{23}NO_3$	314.1751	314.1788	-11.91	9	283, 269	Armepavine isomer	[37]
5	$[M+H]^+$	9.8	$C_{37}H_{40}N_2O_6$	609.2959	609.3011	-8.53	19	578, 547, 206	Berbamine	[38]
6	$[M+H]^+$	10.59	$C_{21}H_{25}NO_4$	356.1856	356.1883	-7.5	10	311, 296, 279	Tetrahydropalmatine	[39]
7	$[M+H]^+$	11.3	$C_{38}H_{42}N_2O_6$	623.3116	623.3159	-6.97	19	592, 549, 206	Pakistanamine	[40]
8	$[M+H]^+$	11.7	$C_{19}H_{17}NO_4$	324.1230	324.1258	-8.56	12	309, 294, 280, 266	Stylopine	[35]
9	$[M+H]^+$	13.2	$C_{20}H_{20}O_4N$	338.1385	338.1384	0.84	12	323, 308, 294, 279	Jatrorrhizine	[41]
10	$[M+H]^+$	13.9	$C_{19}H_{15}NO_4$	322.1074	322.1085	-3.47	13	307, 294, 279	Berberrubine	[42]
11	**$[M+H]^+$**	**14.2**	**$C_{21}H_{22}O_4N$**	**352.1543**	**352.1577**	**-9.58**	**12**	**337, 322, 308, 294**	**Palmatine**	[36]
12	$[M+H]^+$	22.8	$C_{20}H_{17}NO_4$	336.1230	336.1240	-2.88	13	321, 304, 292 279, 263	Berberine	[41]

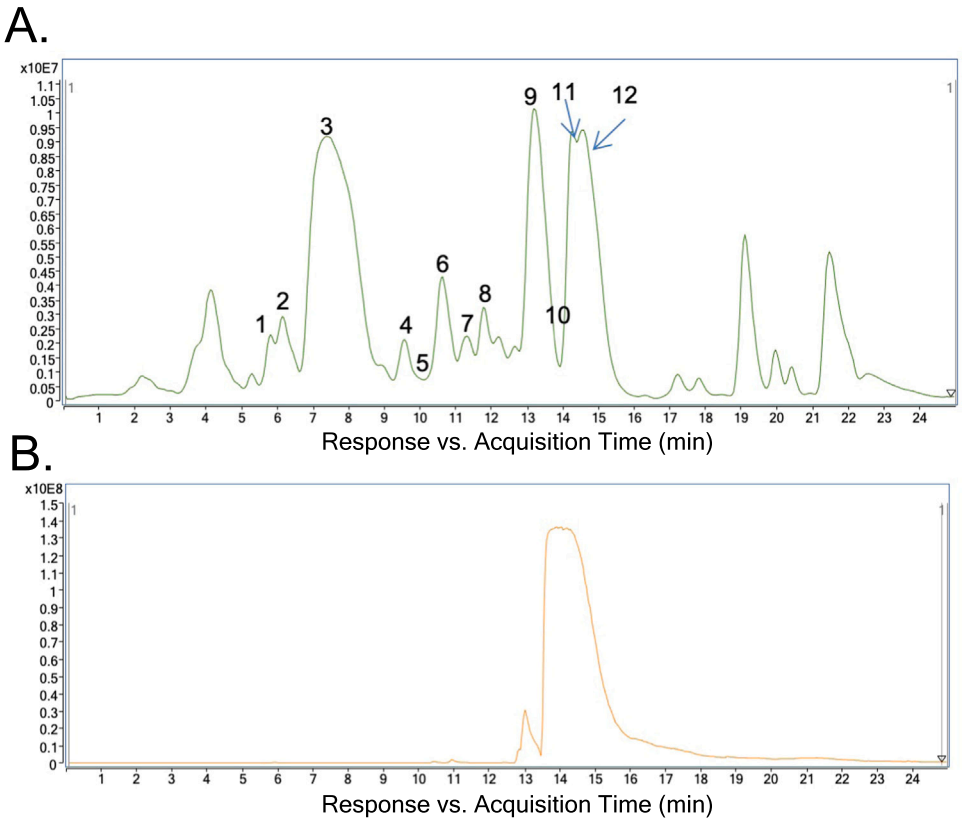

Fig. 1. The total ion chromatogram of the methanolic extract from the roots of *Berberis sibirica.* A. positive ionization mode and the B. total ion chromatogram of the isolated PAL used for the activity studies.

identified and differentially expressed proteins (DEPs) in all regions were presented in Supplementary File 2. Hence, further analyses were focused on DEPs in the hippocampus and cerebellum regions of the PAL2 group's brain.

Unbiased PCA analysis demonstrated the extensive alteration of proteins between the ALM, ALZ, and PAL2 groups in both hippocampus and cerebellum which were evidently separated with principal components 1 (89.9 %) and principal components 2 (8.8 %) in the former (Fig. 4A) and principal components 1 (60.6 %) and principal components 2 (26.9 %) in the latter (Fig. 5A). The samples in the same groups were gathered closely showing good reproducibility.

For a better understanding of the PAL's effect on AD, a pairwise comparison was performed. In the hippocampus, all DEPs identified in PAL2 (compared to ALZ) were also found to be altered in the ALZ (compared to ALM) (Fig. 4B). On the other hand, in the cerebellum out of the 110 DEPs that were detected in PAL2 (compared to ALZ), 58 of them overlapped with those of in ALZ (compared to ALM) (Fig. 5B). These DEPs were further assessed with heatmap, 8 DEPs (100 %) in the hippocampus and 46 (79 %) DEPs in the cerebellum were either low in the ALM, increased in ALZ then decreased in PAL2; or high in the ALM, decreased in ALZ then increased in PAL2 (Fig. 4C-Fig. 5C).

Then, functional annotations and enrichments of those DEPs were performed with Gene Ontology (GO) which provides interpretations of the proteins' biological functions with three ontologies: biological process (BP), molecular function (MF), and cellular component (CC). The top 5 terms in each ontology are presented in the bubble chart the hippocampus (Fig. 6A) and cerebellum (Fig.6B).

The top 3 MFs that DEPs are primarily enriched in were transition metal ion binding, Aβ binding, and identical protein binding in the hippocampus with glutamate decarboxylase activity, glutamate binding, and protein binding in the cerebellum. In GO-BP, DEPs were taking part in the regulation of response to oxidative stress, neuromuscular process

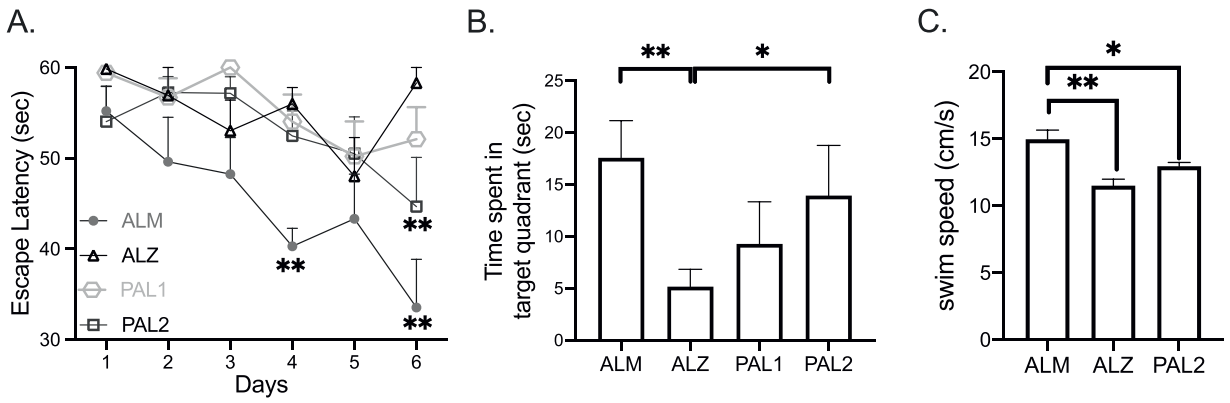

Fig. 2. PAL's effect on spatial learning and memory of 12-month-old 5xFAD mice. A. Escape latency of Alzheimer's Littermate (ALM), 5xFAD Alzheimer's mouse model (ALZ), PAL-5 mg/kg (PAL1), and PAL-10 mg/kg (PAL2) groups. B. Swimming duration in the target quadrant during the probe phase. C. Swim speed of mice across the groups. The data were presented in column bar graph mean ± standard error of the mean (SEM). * ($p < .05$), * * ($p < .01$).

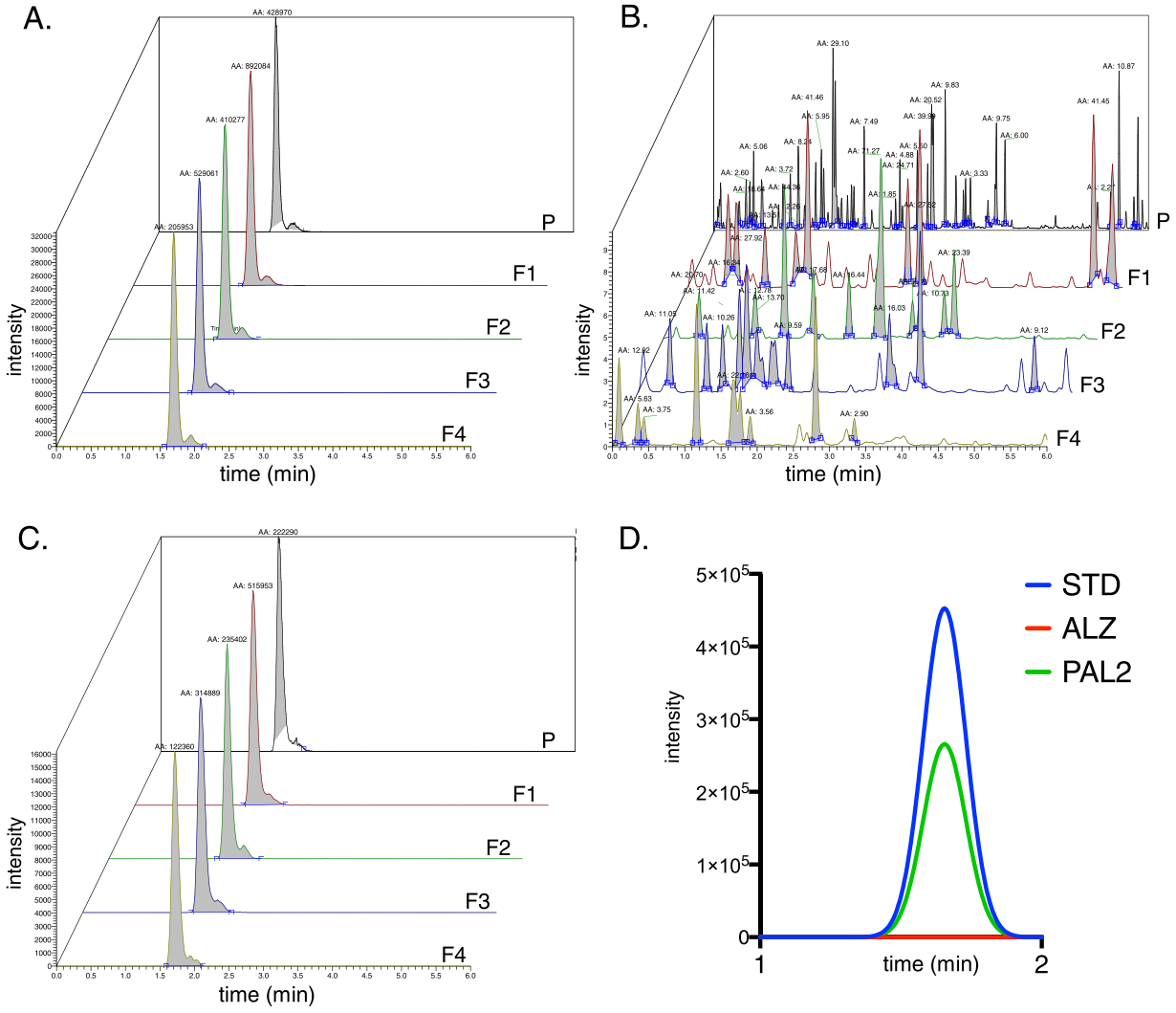

Fig. 3. PAL is able to pass through BBB. Intensity values of TSQ MS analysis of A. pure PAL, brain tissue section of B. ALZ, and C. PAL2. For all Figs. P represents precursor peak of PAL (*m/z*: 352), and F1 (*m/z*: 336), F2 (*m/z*: 337), F3 (*m/z*: 308), F4 (*m/z*: 322) represent fragment ions. D. A representative graph of overlapped intensity values of the PAL at the same retention time.

controlling balance and cholesterol metabolic process pathways in hippocampus and cell proliferation, substantia nigra development, and negative regulation of intrinsic apoptotic signaling pathway in response to hydrogen peroxide pathways in the cerebellum. DEPs were mostly CCs of the extracellular exosome, lysosome, and extracellular space in the hippocampus, on the other hand in the cerebellum they were components of the myelin sheath, extracellular exosome, and focal adhesion (Fig. 6).

Table 2
The number of identified and differentially expressed proteins (DEPs) in cortex, hippocampus, and cerebellum in 5xFAD Alzheimer's model (ALZ) group in comparison to healthy (ALM) group and 10 mg/kg PAL injected (PAL2) 5xFAD group compared to ALZ group.

Regions	Groups	Identified	DEPs	Upregulated	Downregulated
cortex	ALZ/ ALM	1704	252	87	166
	PAL2/ ALZ		0	0	0
hippocampus	ALZ/ ALM	1656	101	20	81
	PAL2/ ALZ		8	2	6
cerebellum	ALZ/ ALM	1478	296	32	264
	PAL2/ ALZ		110	59	51

By KEGG, a database to comprehend the functions and utilities of biological systems, DEPs were found to be enriched in AD pathways in the hippocampus, also in the cerebellum top enriched pathways included the other neurodegenerative diseases (Parkinson's disease (PD), Huntington's disease (HD)) and nervous system (GABAergic synapse) pathways (Fig. 6).

Additionally, protein-protein interaction analysis was performed to identify core regulatory genes. Among 46 proteins determined in the cerebellum, HS105, HS12A, and RL12 were appointed as the top 3 hub proteins via both LAC and DMNC methods (Fig. 7).

3.5. LC-MS/MS analysis validations by Western blot

For the validation of nLC-MS/MS results, the top 3 hub proteins were chosen for the Western blot analyses. Statistical differences were assessed as described in the methods. Western blot analyses showed that HS105 was statistically significantly reduced in ALZ ($t(4) = 8.216$, $p = .0012$) in comparison to ALM, while increased in PAL2 ($t(4) = 6.458$, $p = .003$) compared to ALZ. RL12 showed significant decrease in ALZ ($t(4) = 3.202$, $p = .0328$) compared to ALM and increase in PAL2 ($t(4) = 2.951$, $p = .0419$) against the ALZ. These results are consistent with data obtained by nLC-MS/MS analyses and support the hypothesis that PAL likely recovers the proteomic alterations caused by AD in 5xFAD mouse brains (Fig. 8).

4. Discussion

AD is a progressive neurodegenerative disorder with dramatic degradation of cognitive, social, and emotional function [1]. There are only a few medications for AD which provide symptomatic relief [1,43] or one controversial disease-modifying drug [44]. Therefore, the need for the treatment of AD continues to be a sought-after goal.

Isoquinoline alkaloids are interesting metabolites that have remarkable medicinal implications including neuroprotective functions. Berberine, one of the isoquinoline alkaloids, is the best studied and most widespread compound known as a chemotaxonomic marker of the *Ranunculales* order [35]. It was proven that berberine gets involved in a wide range of biological processes including memory-enhancing activity, reducing the formation of Aβ plaques and NFTs, exhibit lipid- and glucose-lowering properties [45]. In light of recent findings, PAL has received considerable attention as a potential compound that is often accompanying berberine in plant extracts and exerts a marked pharmacologic potential which often exceeds the pharmacological action of berberine [46]. The structural similarity of PAL to berberine makes it difficult to separate them from each other and obtain high-purity compounds on a preparative scale. For this reason, a novel isolation technique, namely CPC was applied in the study and succeeded in the recovery of the compound of interest from the rich matrix of *Berberis sibirica* quantities sufficient in vivo tests. CPC chromatography uses instruments which are equipped in a stainless-steel column with engraved twin cells connected by ducts that play an important role in the affinity-based fractionation of metabolites between the two immiscible solvents as mobile and stationary phases [35]. The application of CPC in the recovery of PAL was especially important due to the fact that isoquinoline alkaloids are capable of irreversible adsorption on classical solid stationary phases which decreases the separation efficiency of the process and also favors the tailing of major components (like berberine) throughout the analysis, leading to decresed purity of the final isolates. Although PAL was isolated by different chromatographic techniques using a hydrodynamic mode of action in the previous studies [47–49], the suggested method in this study was the first method dedicated to

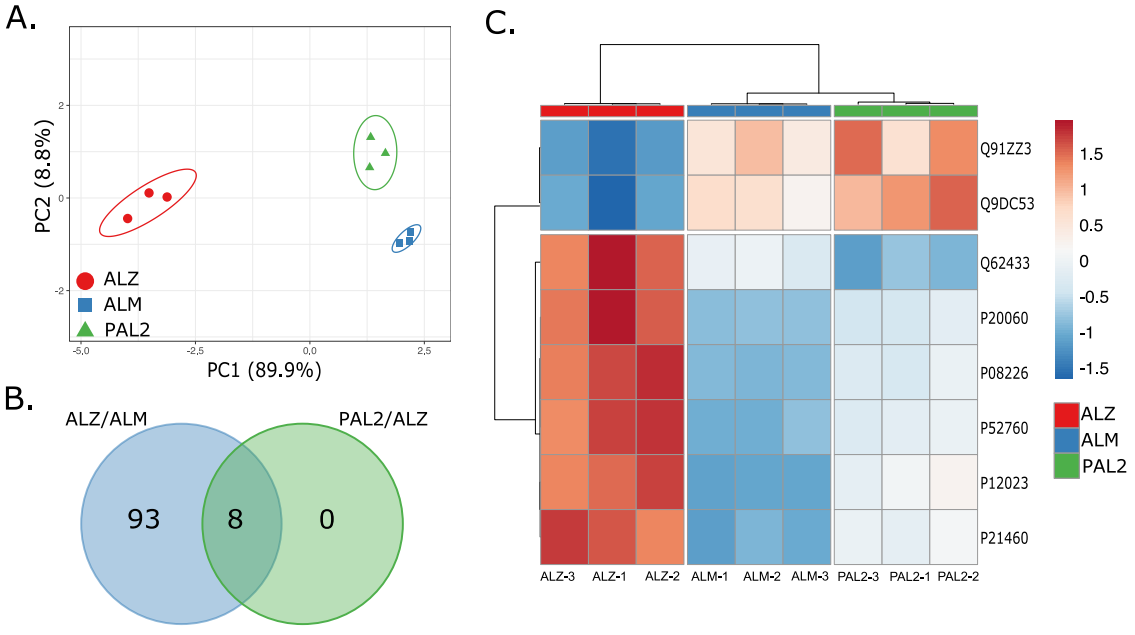

Fig. 4. Systematic bioinformatic analysis of hippocampus. A. PCA analysis, B. Venn scheme reveals commonly altered proteins of ALZ compared to ALM, and PAL2 compared to ALZ groups. C. Heatmap of the abundances of the shared proteins that were detected in the Venn diagram.

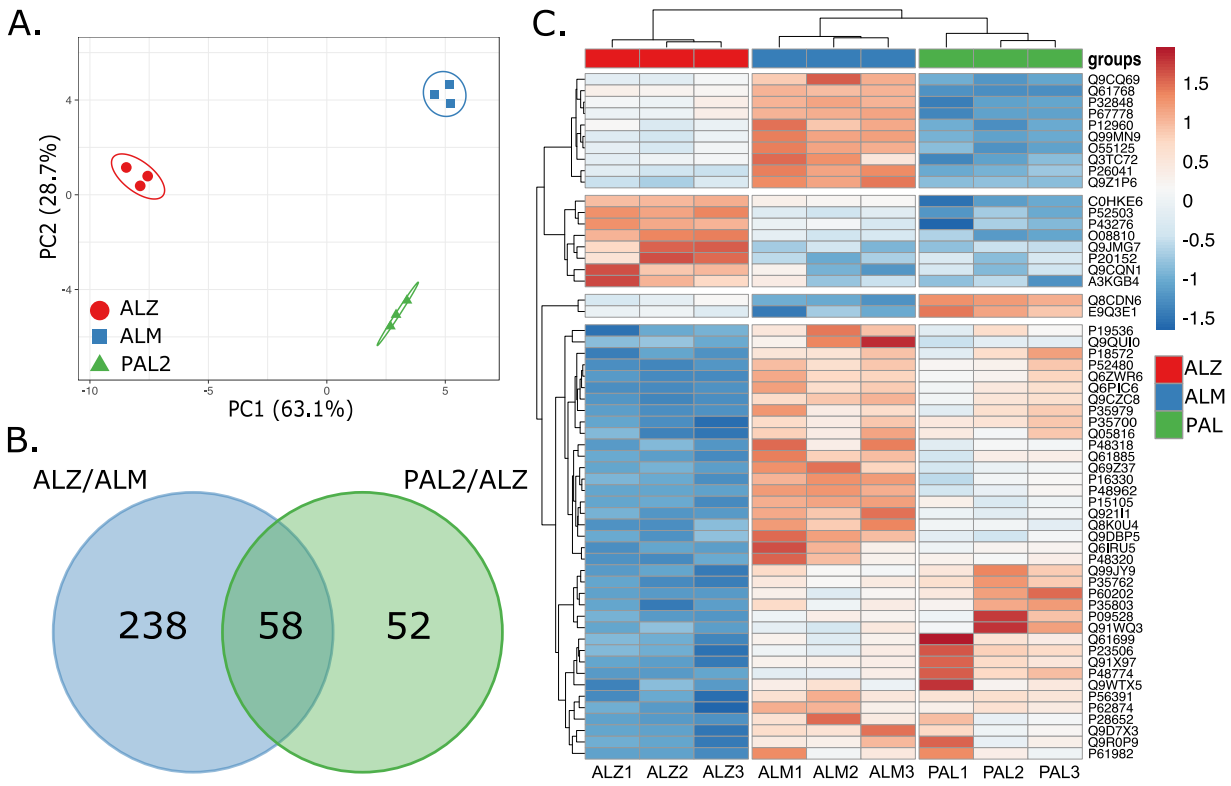

Fig. 5. Systematic bioinformatic analysis of cerebellum. A. PCA analysis, B. Venn scheme reveals commonly altered proteins of ALZ compared to ALM, and PAL2 compared to ALZ groups. C. Heatmap of the abundances of the shared proteins that were detected in the Venn diagram.

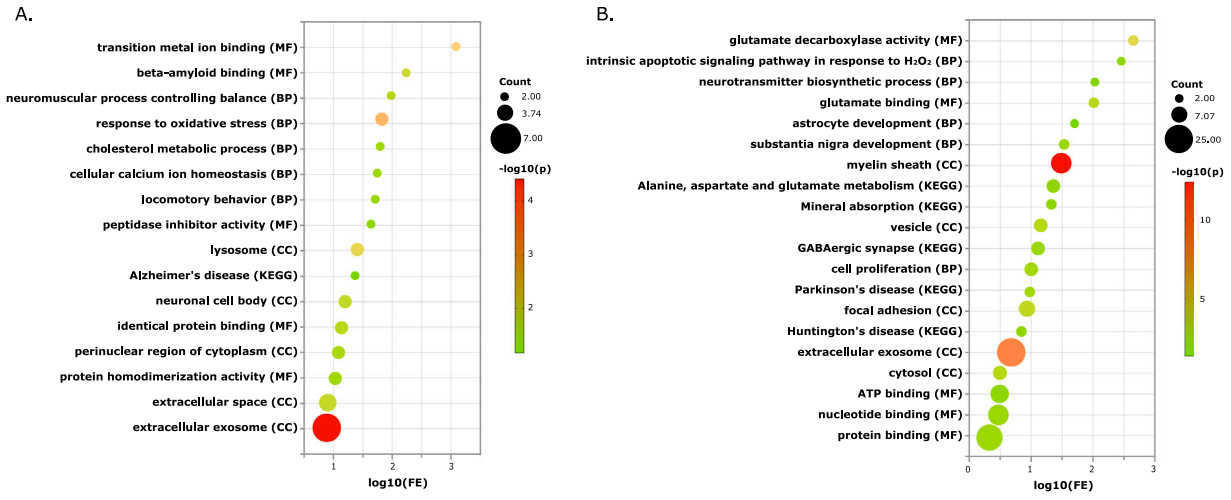

Fig. 6. GO and KEGG enrichment analysis of DEPs. A. hippocampus, B. cerebellum. The y-axis represents GO (MF: Molecular function, BP: Biological process, CC: Cellular component) and KEGG terms, while the x-axis represents fold enrichment (FE). The size of the nodes is proportional to a number of proteins under a specific term (count), and the color represents the *p*-value.

hydrostatic instruments. The herein-described protocol of PAL isolation was successful in that it provided high-purity alkaloids directly from the methanolic extract of *B. sibirica* in a sufficient quantity for the biological activity tests.

5xFAD exerts most of the human AD characteristics [11]; Aβ plaque formation, neuronal loss, synaptic degeneration, gliosis, and memory impairment which are observed at early onset and worsen in an age-dependent manner [2,13,50,51]. 12-month-old 5xFAD was chosen since it shows cognitive impairment and progressed pathological processes and a similar gene/protein expression profile to that of human AD brains [52,53].

Consistent with the literature, we determined the statistically significant decrease in the learning and memory of ALZ (compared to ALM) by MWM test [14,54,55]. On the other hand, in comparison to the ALZ group, the PAL2 group showed significant improvement not only in the learning phase but also in the memory phase. Recently, it has been revealed that after 10 months, 5xFAD shows motor impairment [54,56], which might confound the cognitive performance results. Therefore, we also checked the swim speed, which was statistically decreased in ALZ in comparison to ALM. Even though the velocity of mice was slightly higher after PAL treatment, we could not detect any statistical changes. Therefore, we speculate, the improvement that we observe in MWM

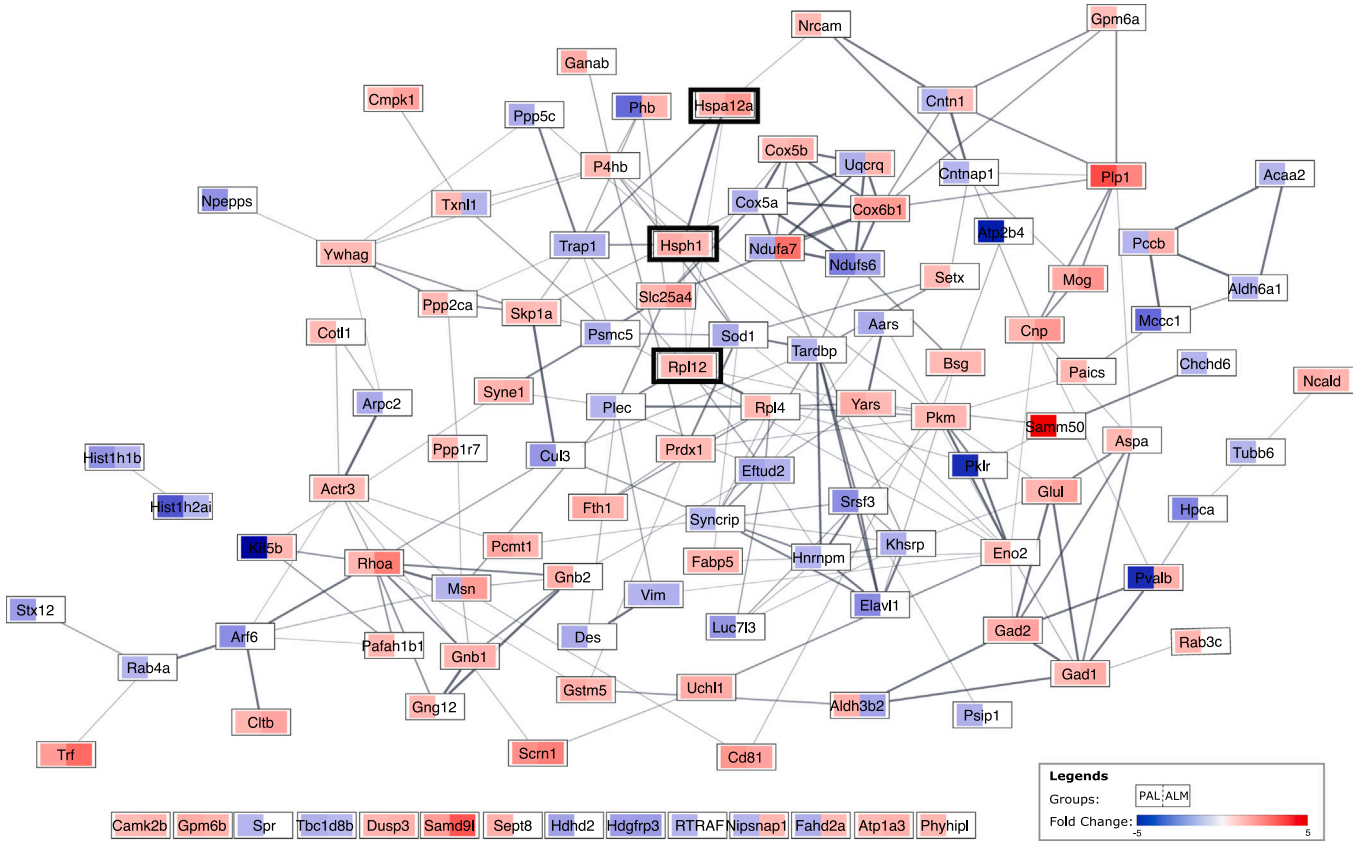

Fig. 7. The protein-protein interaction network map of the DEPs in the ALM and PAL2 groups in comparison to the ALZ group, individually. Representation of ALM in comparison to ALZ was chosen in order to indicate PAL2's ameliorating effect on ALZ. Each node represents a DEP. The left and right side of the rectangle represents the PAL2 vs ALZ, and ALM vs ALZ, respectively. The up-regulation of a DEP was represented in red, and the down-regulation was in blue. The lightness and darkness of the color change gradually due to the fold change (min: −5, max: 5). The white color indicates that protein is not differentially expressed in the given group. The top 3 hub DEPs were indicated with thick black boxes. (Gene names of HS105, HS12A, and RL12 are Hsph1, Hspa12a, and Rpl12, respectively).

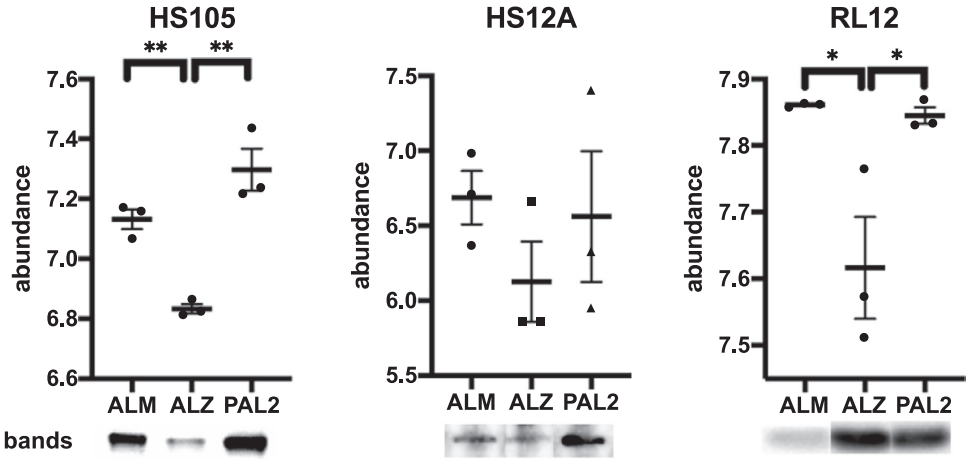

Fig. 8. Western blot analysis of top 3 hub proteins. Data presented with scatter plot graph, mean ± *SEM* of 3 mice cerebellums that each represented with a dot, right under the graph representative band images of each protein was placed. Total protein normalization was performed, and statistical significance set at $p < .05$ (*), $p < .01$ (**).

reflects the learning and memory ability of the mice. Also, as in the other neurodegenerative diseases, (HD, PD) motor and cognitive deficits can occur simultaneously and an effective therapy can target and improve both functions [57].

The BBB is the primary obstacle to most of the drugs that target especially central nervous system disorders. Following that the BBB penetration of PAL was proved by MRM-MS analysis which was corroborated by earlier studies [22,58]. The underlying molecular mechanism of PAL (10 mg/kg) that led to improvement of cognition was investigated via label-free MS analysis. The pairwise comparison was carried out between PAL2 versus ALZ and ALZ versus ALM groups. This approach aimed to reveal PAL2's effects on AD-induced changes in 5xFAD mice by eliminating alterations caused by other parameters. Diseases and therapeutics affect the brain regionally through the

magnitude and direction of changes in abundance [59]. Therefore, proteomics analysis was carried out on the cortex, hippocampus, and cerebellum, individually. Interestingly, the cerebellum was found to be a prominently affected brain region by PAL2 in addition to minor alterations in the hippocampus. The most striking result to emerge from both regions' data is that the proteins decreased in AD were increased again (or vice versa) following PAL2 administration, which makes PAL a strong potential therapeutic agent.

Hippocampus is the part of the brain that is critical for learning, memory, and stores long-term memories. Dysfunctions in the hippocampus are thought to contribute greatly to memory impairment in AD [60]. GO analysis indicated that DEPs in the hippocampus of PAL2 were most significantly enriched in response to oxidative stress, transition metal ion binding, and Aβ binding pathways, which are known to be highly associated with each other and AD. KEGG analysis also supported this finding by revealing that DEPs were enriched in the AD pathway. The increase of oxidative stress in AD, shown by many studies, pointed out its early-stage involvement in the disease's mechanism [61–63]. Even some theories suggested the major hallmarks of AD, Aβ, and NFTs were formed to compensate for the oxidative stress [64], oxidative damage is found to be positively correlated with the amount of the Aβ plaques [64,65]. Furthermore, Aβ and its precursor APP have been associated with biometals through their high-affinity binding sites [66–68]. Copper was detected in Aβ plaques in high concentrations. It also plays role in oxidative stress in AD as a mediator of reactive hydroxy radicals [69,70]. Similarly increased concentrations of zinc were detected in memory and cognition-related parts of the brain, exclusively in the hippocampus [71]. This increase was associated with oxidative stress induced by the uncontrolled accumulation of zinc and Aβ [72]. Therefore, PAL2-induced alterations in the hippocampus through the aforementioned pathways might contribute to the reversal of the learning and memory of AD mice.

Compared to the hippocampal formation, the cerebellum was thought to be a silent bystander in AD. However, recent studies implicated the cerebellum as playing an active role in AD through undergoing structural, functional, and degenerative changes [73–78]. The cerebellar volume, which was reduced with the severity of dementia [79], is correlated with cognitive function, memory, and thought organization [74–77,80]. Two recent genome-wide association studies pointed out that intelligence and cognitive function-related genes were mostly expressed in the cerebellum, along with the cortex [81,82] and these genes were enriched in similar pathways as those in our study. GO analysis in our research showed that DEPs were mostly associated with cell proliferation, glutamate binding, and glutamate decarboxylase activity. In AD, cell proliferation in the hippocampus, known as hippocampal neurogenesis, was reported to be inhibited by Aβ [83]. Glutamate is the primary excitatory neurotransmitter in the CNS which plays an important role in learning and memory. Glutamic acid decarboxylase 1 (DCE1; GN=GAD1) and glutamic acid decarboxylase 2 (DCE2; GN=GAD2) which synthesize the principal inhibitory neurotransmitter GABA [84] and glutamine synthetase (GLNA, GN=Glul) which converts glutamate to glutamine to be used by neurons were reported to be downregulated in AD [85,86]. Another remarkable outcome of this study was that the expression levels of these proteins were upregulated again by PAL2.

KEGG pathway analysis revealed that DEPs were enriched in other neurodegenerative diseases: Parkinson's disease (PD) and Huntington's disease (HD). PD is known for motor dysfunctions, and its underlying mechanism is associated with basal ganglia. However, just as in AD, in recent years researchers have been pointing out the importance of the cerebellum through its pathophysiological and compensatory mechanisms in HD [87–89]. Neurodegenerative diseases shared common properties such as being progressive and debilitating, instigated by the death of brain cells, and their mechanisms involve aggregated/misfolded proteins [90].

In an effort to reveal key proteins among DEPs, we applied two commonly used and advised protein-protein interaction analysis methods together, LAC and DMNC. In agreement, these methods indicated HS105, HS12A, and RL12 as the top 3 hub proteins. All 3 proteins were found to be downregulated in ALZ compared to ALM and upregulated in PAL2 compared to ALZ. Hence, we can suggest that AD's effect on these proteins' expressions was mitigated by PAL2. This finding further supports these proteins as being key players. In order to reveal the association of these proteins to AD, their roles will be briefly mentioned below.

HS105 (Heat shock protein 105 kDa), an isoform of heat shock protein 110, is a part of the major disaggregase machinery in mammalians [91]. HS105 is shown to be the main player in refolding the misfolded proteins to their native state and protecting the cell against stress-induced cell death [92,93]. Loss of HS105 in mice caused tau hyperphosphorylation and early accumulation of Aβ [94]. HS105 also collaborates with our other hub protein HS12A to form powerful chaperone machinery which can unfold and solubilize misfolded and aggregated proteins [95]. HS12A (Heat shock 70 kDa protein 12 A) is a member of the HSP70 family, reported having neuroprotective activity [96]. Even though information about its function is scarce, HS12A was identified as an exclusive adaptor protein for SorLa, which is a cargo molecule that carries amyloid protein to where they are broken down [97]. RL12 (60 S ribosomal protein L12) is a component of the large subunit (60 S) of the ribosome. The expression of various ribosomal proteins (RPLs) was reported to be changed in the brains of mice and patients with AD, pointing out the altered protein synthesis machinery in AD [98–100]. RL12 is significantly altered in between blood and brain in the AD mouse [101]. A network-based computational study suggested RL12 as one of the key signaling and regulatory molecules in AD [102]. Re-regulation of these proteins in PAL2 might play essential role in the restoration of the learning and memory abilities of 12-month-old 5xFAD mice model.

In recent years, researchers have been suggesting that combination therapies have a greater capacity for the treatment of multifactorial disease AD [103,104]. Our recent work showed galantamine, FDA approved AD drug, and several other alkaloids and coumarins exerted their effect in the cortex, prominently [23,24]. Whereas here, PAL mainly targeted the cerebellum. Therefore, we can suggest that PAL can be further evaluated/investigated as a part of combination therapy.

5. Conclusions

In summary, PAL's potential therapeutic effect was evaluated on the AD mouse model. After isolation and 7-day administration of PAL (10 mg/kg) to 12-month-old 5xFAD mice, statisticallysignificant improvements in learning and memory were detected via the MWM test. BBB passage was proven with MRM analysis. The underlying mechanism which led to improvement in cognition was investigated by nLC-MS/MS in the cortex, hippocampus, and cerebellum of the brain. Surprisingly, the cerebellum was the prominent site of the alterations in PAL. A pairwise comparison of the DEPs revealed that most of the changes in PAL compared to ALZ were opposite of those in ALZ in comparison to ALM. Bioinformatic analyses revealed HS105, HS12A, and RL12 proteins as hub proteins, and their protein expression levels were verified with Western blot analysis. Collectively, here we present PAL as a potential therapeutic candidate owing to its alleviating effect in 5xFAD mice on not only cognitive impairment but also proteomes in the cerebellum and hippocampus. Also, we speculate that PAL might be a good candidate for combination therapies since it distinctively targets the cerebellum.

Funding statement

This work was supported by TUBITAK (Turkey) – NCBR (Poland) Bilateral Cooperation Program [215S168, 4/POLTUR-1/2016]; the Acibadem University Scientific Research Projects Commission

[ABAPKO, 2022/01-30], and the Medical University of Lublin [DS24].

Ethics approval

All animal procedures have been approved by the Ethics Committee of the Animal Care and Use Committee of Acibadem Mehmet Ali Aydinlar University, Istanbul, Turkey (Approval ID: 2016/7). All institutional and national guidelines for the care and use of laboratory animals were followed.

Consent to participate

Not applicable.

Consent for publication

Not applicable.

Code availability

Not applicable.

CRediT authorship contribution statement

Irem Kiris: Formal analysis, Investigation, Validation, Visualization, Writing – original draft, Writing – review & editing. **Wirginia Kukula-Koch:** Project administration, Funding acquisition, Investigation, Writing – original draft, Writing – review & editing. **Merve Karayel-Basar:** Investigation, Writing – review & editing. **Busra Gurel:** Investigation, Writing – review & editing. **Ahmet Tarik Baykal:** Project administration, Funding acquisition, Supervision.

Conflict of interest statement

The authors declare that there are no conflicts of interest.

Data availability

All data generated or analyzed during this study are included in this published article [and its supplementary information files]. Further information can be requested from the corresponding author.

Acknowledgements

The authors of the manuscript would like to thank Dr. Otgonbataar Urjin from the Mongolian National University of Medical Sciences for providing plant material for the isolation of PAL.

Appendix A. Supporting information

Supplementary data associated with this article can be found in the online version at doi:10.1016/j.biopha.2022.114111.

References

[1] Gauthier S., Rosa-Neto P., Morais J.A., Webster C. , 2021, World Alzheimer Report 2021: Journey Through the Diagnosis of Dementia. London, England.
[2] A. Armstrong R, Plaques and tangles and the pathogenesis of Alzheimer's disease, Folia Neuropathol. 44 (2006) 1–11.
[3] S.S. Mirra, A. Heyman, D. McKeel, et al., The Consortium to Establish a Registry for Alzheimer's Disease (CERAD): part II. Standardization of the neuropathologic assessment of Alzheimer's disease, Neurology 41 (1991) 479, https://doi.org/10.1212/WNL.41.4.479.
[4] R.R. Tampi, B.P. Forester, M. Agronin, Aducanumab: evidence from clinical trial data and controversies, Drugs Context 10 (2021).
[5] J. Long, J. Song, L. Zhong, et al., Palmatine: a review of its pharmacology, toxicity and pharmacokinetics, Biochimie 162 (2019) 176–184.
[6] W. Kukula-Koch, T. Mroczek, Application of hydrostatic CCC–TLC–HPLC–ESI-TOF-MS for the bioguided fractionation of anticholinesterase alkaloids from Argemone mexicana L. roots, Anal. Bioanal. Chem. 407 (2015) 2581–2589, https://doi.org/10.1007/s00216-015-8468-x.
[7] H.A. Jung, B.-S. Min, T. Yokozawa, et al., Anti-Alzheimer and antioxidant activities of Coptidis Rhizoma alkaloids, Biol. Pharm. Bull. 32 (2009) 1433–1438, https://doi.org/10.1248/bpb.32.1433.
[8] E. Haj, Y. Losev, V. Guru KrishnaKumar, et al., Integrating in vitro and in silico approaches to evaluate the "dual functionality" of palmatine chloride in inhibiting and disassembling Tau-derived VQIVYK peptide fibrils, Biochim. Biophys. Acta Gen. Subj. 1862 (2018) 1565–1575, https://doi.org/10.1016/j.bbagen.2018.04.001.
[9] D. Dhingra, V. Kumar, Memory-enhancing activity of palmatine in mice using elevated plus maze and Morris water maze, Adv. Pharmacol. Sci. (2012) 2012, https://doi.org/10.1155/2012/357368.
[10] S. Forner, S. Kawauchi, G. Balderrama-Gutierrez, et al., Systematic phenotyping and characterization of the 5xFAD mouse model of Alzheimer's disease, Sci. Data 8 (2021), https://doi.org/10.1038/s41597-021-01054-y.
[11] H. Sasaguri, P. Nilsson, S. Hashimoto, et al., APP mouse models for Alzheimer's disease preclinical studies, EMBO J. 36 (2017) 2473–2487, https://doi.org/10.15252/embj.201797397.
[12] S. Jawhar, A. Trawicka, C. Jenneckens, et al., Motor deficits, neuron loss, and reduced anxiety coinciding with axonal degeneration and intraneuronal Aβ aggregation in the 5XFAD mouse model of Alzheimer's disease, Neurobiol. Aging 33 (2012) 196.e29–196.e40, https://doi.org/10.1016/j.neurobiolaging.2010.05.027.
[13] M. Ohno, L. Chang, W. Tseng, et al., Temporal memory deficits in Alzheimer's mouse models: rescue by genetic deletion of BACE1, Eur. J. Neurosci. 23 (2006) 251–260, https://doi.org/10.1111/j.1460-9568.2005.04551.x.
[14] H. Oakley, S.L. Cole, S. Logan, et al., Intraneuronal β-amyloid aggregates, neurodegeneration, and neuron loss in transgenic mice with five familial Alzheimer's disease mutations: potential factors in amyloid plaque formation, J. Neurosci. 26 (2006) 10129–10140, https://doi.org/10.1523/JNEUROSCI.1202-06.2006.
[15] B. Gurel, M. Cansev, C. Koc, et al., Proteomics analysis of CA1 region of the hippocampus in pre-, progression and pathological stages in a mouse model of the Alzheimer's disease, Curr. Alzheimer Res. 16 (2019) 613–621, https://doi.org/10.2174/1567205016666190730155926.
[16] Y. Bouter, T. Kacprowski, R. Weissmann, et al., Deciphering the molecular profile of plaques, memory decline and neuron loss in two mouse models for Alzheimer's disease by deep sequencing, Front Aging Neurosci. 6 (2014), https://doi.org/10.3389/fnagi.2014.00075.
[17] V. Landel, K. Baranger, I. Virard, et al., Temporal gene profiling of the 5XFAD transgenic mouse model highlights the importance of microglial activation in Alzheimer's disease, Mol. Neurodegener. 9 (2014) 1–18, https://doi.org/10.1186/1750-1326-9-33.
[18] E. Drummond, T. Wisniewski, Using proteomics to understand alzheimer's disease pathogenesis, Alzheimer's Dis. (2019) 37–51, https://doi.org/10.15586/alzheimersdisease.2019.ch3.
[19] M. Frantzi, A. Latosinska, H. Mischak, Proteomics in drug development: the dawn of a new era? Proteom. Clin. Appl. 13 (2019) 1800087, https://doi.org/10.1002/prca.201800087.
[20] Z. Li, R.M. Adams, K. Chourey, et al., Systematic comparison of label-free, metabolic labeling, and isobaric chemical labeling for quantitative proteomics on LTQ orbitrap velos, J. Proteome Res. 11 (2012) 1582–1590, https://doi.org/10.1021/pr200748h.
[21] T.J. Montine, R.L. Woltjer, C. Pan, et al., Liquid chromatography with tandem mass spectrometry-based proteomic discovery in aging and Alzheimer's disease, NeuroRx 3 (2006) 336–343, https://doi.org/10.1016/j.nurx.2006.05.002.
[22] K. Gawel, W. Kukula-Koch, D. Nieoczym, et al., The influence of palmatine isolated from berberis sibirica radix on pentylenetetrazole-induced seizures in zebrafish, Cells 9 (2020) 1233, https://doi.org/10.3390/cells9051233.
[23] I. Kiris, M.K. Basar, B. Sahin, et al., Evaluation of the therapeutic effect of lycoramine on Alzheimer's disease in mouse model, Curr. Med. Chem. 28 (2021) 3449–3473, https://doi.org/10.2174/0929867327999201116193126.
[24] I. Kiris, K. Skalicka-Wozniak, M.K. Basar, et al., Molecular effects of pteryxin and scopoletin in the 5xFAD Alzheimer's disease mouse model, Curr. Med. Chem. 29 (2022) 2937–2950, https://doi.org/10.2174/0929867328666210827152914.
[25] J.R. Wiśniewski, A. Zougman, N. Nagaraj, M. Mann, Universal sample preparation method for proteome analysis, Nat. Methods 6 (2009) 359–362, https://doi.org/10.1038/nmeth.1322.
[26] M.A. Moseley, C.J. Hughes, P.R. Juvvadi, et al., Scanning quadrupole data-independent acquisition, part a: qualitative and quantitative characterization, J. Proteome Res. 17 (2018) 770–779, https://doi.org/10.1021/acs.jproteome.7b00464.
[27] T. Metsalu, J. Vilo, ClustVis: a web tool for visualizing clustering of multivariate data using principal component analysis and heatmap, Nucleic Acids Res. 43 (2015) W566–W570, https://doi.org/10.1093/nar/gkv468.
[28] D.W. Huang, B.T. Sherman, R.A. Lempicki, Systematic and integrative analysis of large gene lists using DAVID bioinformatics resources, Nat. Protoc. 4 (2009) 44–57, https://doi.org/10.1038/nprot.2008.211.
[29] D.W. Huang, B.T. Sherman, R.A. Lempicki, Bioinformatics enrichment tools: paths toward the comprehensive functional analysis of large gene lists, Nucleic Acids Res. 37 (2009) 1–13, https://doi.org/10.1093/nar/gkn923.
[30] P. Shannon, A. Markiel, O. Ozier, et al., Cytoscape: a software environment for integrated models of biomolecular interaction networks, Genome Res. 13 (2003) 2498–2504, https://doi.org/10.1101/gr.1239303.

[31] D. Szklarczyk, J.H. Morris, H. Cook, et al., The STRING database in 2017: quality-controlled protein-protein association networks, made broadly accessible, Nucleic Acids Res. 45 (2017) D362–D368, https://doi.org/10.1093/nar/gkw937.
[32] Y. Tang, M. Li, J. Wang, et al., CytoNCA: a cytoscape plugin for centrality analysis and evaluation of protein interaction networks, Biosystems 127 (2015) 67–72, https://doi.org/10.1016/j.biosystems.2014.11.005.
[33] C.-H. Chin, S.-H. Chen, H.-H. Wu, et al., cytoHubba: identifying hub objects and sub-networks from complex interactome, BMC Syst. Biol. 8 (2014) S11, https://doi.org/10.1186/1752-0509-8-S4-S11.
[34] A. Kumar, Ekavali, K. Chopra, et al., Current knowledge and pharmacological profile of berberine: an update, Eur. J. Pharmacol. 761 (2015) 288–297, https://doi.org/10.1016/j.ejphar.2015.05.068.
[35] W. Kukula-Koch, The elevation of LC-ESI-Q-TOF-MS response in the analysis of isoquinoline alkaloids from some papaveraceae and berberidaceae representatives, J. Anal. Methods Chem. 2017 (2017) 1–9, https://doi.org/10.1155/2017/8384107.
[36] X. Tian, Z. Li, Y. Lin, et al., Study on the PK profiles of magnoflorine and its potential interaction in Cortex phellodendri decoction by LC-MS/MS, Anal. Bioanal. Chem. 406 (2014) 841–849, https://doi.org/10.1007/s00216-013-7530-9.
[37] P. Geng, J. Luo, Z. Weng, et al., Determination of armepavine in mouse blood by UPLC-MS/MS and its application to pharmacokinetic study, Biomed. Chromatogr. (2018), e4273, https://doi.org/10.1002/bmc.4273.
[38] A. Hostalkova, J. Marikova, L. Opletal, et al., Isoquinoline alkaloids from *Berberis vulgaris* as potential lead compounds for the treatment of Alzheimer's disease, J. Nat. Prod. 82 (2019) 239–248, https://doi.org/10.1021/acs.jnatprod.8b00592.
[39] J.W. Jung, Y.S. Kwon, J.S. Jeong, et al., Pharmacokinetics and brain distribution of tetrahydropalmatine and tetrahydroberberine after oral administration of DA-9701, a new botanical gastroprokinetic agent, in rats, Biol. Pharm. Bull. 38 (2015) 285–291, https://doi.org/10.1248/bpb.b14-00678.
[40] V. Bajpai, A. Singh, K.R. Arya, et al., Rapid screening for the adulterants of Berberis aristata using direct analysis in real-time mass spectrometry and principal component analysis for discrimination, Food Addit. Contam. Part A 32 (2015) 799–807, https://doi.org/10.1080/19440049.2015.1022885.
[41] E. Plazas, R. Casoti, M. Avila Murillo, et al., Metabolomic profiling of Zanthoxylum species: identification of anti-cholinesterase alkaloids candidates, Phytochemistry 168 (2019), 112128, https://doi.org/10.1016/j.phytochem.2019.112128.
[42] Y. Zhao, N. Yang, F. Fei, et al., Sensitive analysis and pharmacokinetic study of berberrubine using LC-MS/MS, Chin. Herb. Med. 9 (2017) 236–249, https://doi.org/10.1016/S1674-6384(17)60100-X.
[43] K. Yamada, T. Nabeshima, Animal models of Alzheimer's disease and evaluation of anti-dementia drugs, Pharmacol. Ther. 88 (2000) 93–113, https://doi.org/10.1016/S0163-7258(00)00081-4.
[44] J. Sevigny, P. Chiao, T. Bussière, et al., The antibody aducanumab reduces Aβ plaques in Alzheimer's disease, Nature 537 (2016) 50–56, https://doi.org/10.1038/nature19323.
[45] Z. Cai, C. Wang, W. Yang, Role of berberine in Alzheimer's disease, Neuropsychiatr. Dis. Treat. Volume 12 (2016) 2509–2520, https://doi.org/10.2147/NDT.S114846.
[46] D. Tarabasz, W. Kukula-Koch, Palmatine: a review of pharmacological properties and pharmacokinetics, Phytother. Res. 34 (2020) 33–50, https://doi.org/10.1002/ptr.6504.
[47] F. Yang, T. Zhang, R. Zhang, Y. Ito, Application of analytical and preparative high-speed counter-current chromatography for separation of alkaloids from Coptis chinensis Franch, J. Chromatogr. A 829 (1998) 137–141, https://doi.org/10.1016/S0021-9673(98)00776-6.
[48] S. Zhang, M. Wang, C. Wang, Preparative separation and purification of alkaloids from Rhizoma coptidis by high-speed counter-current chromatography, Sep Purif. Technol. 76 (2011) 428–431, https://doi.org/10.1016/j.seppur.2010.10.019.
[49] S. Tong, J. Yan, J. Lou, Preparative isolation and purification of alkaloids from *Corydalis yanhusuo* W. T. Wang by high speed counter-current chromatography, J. Liq. Chromatogr. Relat. Technol. 28 (2005) 2979–2989, https://doi.org/10.1080/10826070500274638.
[50] J.M. Rollinger, A. Hornick, T. Langer, et al., Acetylcholinesterase inhibitory activity of scopolin and scopoletin discovered by virtual screening of natural products, J. Med. Chem. 47 (2004) 6248–6254, https://doi.org/10.1021/jm049655r.
[51] H.C. Lin, S.H. Tsai, C.S. Chen, et al., Structure-activity relationship of coumarin derivatives on xanthine oxidase-inhibiting and free radical-scavenging activities, Biochem. Pharmacol. 75 (2008) 1416–1425, https://doi.org/10.1016/j.bcp.2007.11.023.
[52] C.L. Maarouf, T.A. Kokjohn, C.M. Whiteside, et al., Molecular differences and similarities between Alzheimer's disease and the 5XFAD transgenic mouse model of amyloidosis, Biochem Insights 6 (2013), BCI.S13025, https://doi.org/10.4137/BCI.S13025.
[53] Y. Bouter, T. Kacprowski, R. Weissmann, et al., Deciphering the molecular profile of plaques, memory decline and neuron loss in two mouse models for Alzheimer's disease by deep sequencing, Front. Aging Neurosci. 6 (2014), https://doi.org/10.3389/fnagi.2014.00075.
[54] T.P. O'Leary, R.E. Brown, Visuo-spatial learning and memory impairments in the 5xFAD mouse model of Alzheimer's disease: effects of age, sex, albinism, and motor impairments, Genes Brain Behav. 21 (2022), https://doi.org/10.1111/gbb.12794.
[55] S. Bhattacharya, C. Haertel, A. Maelicke, D. Montag, Galantamine slows down plaque formation and behavioral decline in the 5XFAD mouse model of Alzheimer's disease, PLoS One 9 (2014) 1–12, https://doi.org/10.1371/journal.pone.0089454.
[56] T. O'Leary, A. Robertson, P. Chipman, et al., Motor dysfunction in the 12-month-old 5xFAD mouse model of Alzheimer's disease, Alzheimer's Dement. 9 (2013) P497, https://doi.org/10.1016/j.jalz.2013.05.1027.
[57] H. Liu, S. Li, C. Yang, et al., D-serine ameliorates motor and cognitive impairments in β-amyloid 1-42 injected mice by inhibiting JNK signaling pathway, J. Chem. Neuroanat. 109 (2020), https://doi.org/10.1016/j.jchemneu.2020.101852.
[58] Y. Gao, S. Hu, M. Zhang, et al., Simultaneous determination of four alkaloids in mice plasma and brain by LC–MS/MS for pharmacokinetic studies after administration of Corydalis Rhizoma and Yuanhu Zhitong extracts, J. Pharm. Biomed. Anal. 92 (2014) 6–12, https://doi.org/10.1016/j.jpba.2013.12.037.
[59] J. McKetney, R.M. Runde, A.S. Hebert, et al., Proteomic atlas of the human brain in Alzheimer's disease, J. Proteome Res. 18 (2019) 1380–1391, https://doi.org/10.1021/acs.jproteome.9b00004.
[60] V. Dhikav, K. Anand, Hippocampus in health and disease: an overview, Ann. Indian Acad. Neurol. 15 (2012) 239, https://doi.org/10.4103/0972-2327.104323.
[61] M. Padurariu, A. Ciobica, R. Lefter, et al., The oxidative stress hypothesis in Alzheimer's disease, Psychiatr. Danub 25 (2013) 401–409.
[62] Y. Christen, Oxidative stress and Alzheimer disease, Am. J. Clin. Nutr. 71 (2000) 621S–629S, https://doi.org/10.1093/ajcn/71.2.621s.
[63] B. Gurel, M. Cansev, C. Sevinc, et al., Early stage alterations in CA1 extracellular region proteins indicate dysregulation of IL6 and iron homeostasis in the 5XFAD Alzheimer's disease mouse model, J. Alzheimer's Dis. 61 (2018) 1399–1410, https://doi.org/10.3233/JAD-170329.
[64] A. Nunomura, R.J. Castellani, X. Zhu, et al., Involvement of oxidative stress in Alzheimer disease, J. Neuropathol. Exp. Neurol. 65 (2006) 631–641, https://doi.org/10.1097/01.jnen.0000228136.58062.bf.
[65] W.J. Huang, X. Zhang, W.W. Chen, Role of oxidative stress in Alzheimer's disease (review), Biomed. Rep. 4 (2016) 519–522, https://doi.org/10.3892/br.2016.630.
[66] T. Miura, K. Suzuki, N. Kohata, H. Takeuchi, Metal binding modes of Alzheimer's amyloid β-Peptide in insoluble aggregates and soluble complexes, Biochemistry 39 (2000) 7024–7031, https://doi.org/10.1021/bi0002479.
[67] K.J. Barnham, W.J. McKinstry, G. Multhaup, et al., Structure of the Alzheimer's disease amyloid precursor protein copper binding domain, J. Biol. Chem. 278 (2003) 17401–17407, https://doi.org/10.1074/jbc.M300629200.
[68] H. Kozlowski, A. Janicka-Klos, J. Brasun, et al., Copper, iron, and zinc ions homeostasis and their role in neurodegenerative disorders (metal uptake, transport, distribution and regulation, Coord. Chem. Rev. 253 (2009) 2665–2685, https://doi.org/10.1016/j.ccr.2009.05.011.
[69] D. Strozyk, L.J. Launer, P.A. Adlard, et al., Zinc and copper modulate Alzheimer Aβ levels in human cerebrospinal fluid, Neurobiol. Aging 30 (2009) 1069–1077, https://doi.org/10.1016/j.neurobiolaging.2007.10.012.
[70] M. Valko, H. Morris, M. Cronin, Metals, toxicity and oxidative stress, Curr. Med. Chem. 12 (2005) 1161–1208, https://doi.org/10.2174/0929867053764635.
[71] M.P. Cuajungco, K.Y. Fagét, Zinc takes the center stage: its paradoxical role in Alzheimer's disease, Brain Res. Rev. 41 (2003) 44–56, https://doi.org/10.1016/S0165-0173(02)00219-9.
[72] A. Pal, R.K. Badyal, R.K. Vasishta, et al., Biochemical, histological, and memory impairment effects of chronic copper toxicity: a model for non-wilsonian brain copper toxicosis in Wistar rat, Biol. Trace Elem. Res. 153 (2013) 257–268, https://doi.org/10.1007/s12011-013-9665-0.
[73] H.M. Gellersen, X. Guell, S. Sami, Differential vulnerability of the cerebellum in healthy ageing and Alzheimer's disease, Neuroimage Clin. 30 (2021), https://doi.org/10.1016/j.nicl.2021.102605.
[74] H. Picard, I. Amado, S. Mouchet-Mages, et al., The role of the cerebellum in schizophrenia: an update of clinical, cognitive, and functional evidences, Schizophr. Bull. 34 (2008) 155–172, https://doi.org/10.1093/schbul/sbm049.
[75] T.H. Wassink, N.C. Andreasen, P. Nopoulos, M. Flaum, Cerebellar morphology as a predictor of symptom and psychosocial outcome in schizophrenia, Biol. Psychiatry 45 (1999) 41–48, https://doi.org/10.1016/s0006-3223(98)00175-9.
[76] V. dos Santos, P.A. Thomann, T. Wüstenberg, et al., Morphological cerebral correlates of CERAD test performance in mild cognitive impairment and Alzheimer's disease, J. Alzheimers Dis. 23 (2011) 411–420, https://doi.org/10.3233/JAD-2010-100156.
[77] C.C. Guo, R. Tan, J.R. Hodges, et al., Network-selective vulnerability of the human cerebellum to Alzheimer's disease and frontotemporal dementia, Brain 139 (2016) 1527–1538, https://doi.org/10.1093/brain/aww003.
[78] P.A. Thomann, C. Schläfer, U. Seidl, et al., The cerebellum in mild cognitive impairment and Alzheimer's disease - a structural MRI study, J. Psychiatr. Res. 42 (2008) 1198–1202, https://doi.org/10.1016/j.jpsychires.2007.12.002.
[79] L. Baldaçara, J.G.F. Borgio, W.A. Moraes, S. dos, et al., Cerebellar volume in patients with dementia, Rev. Bras. De. Psiquiatr. 33 (2011) 122–129, https://doi.org/10.1590/S1516-44462011000200006.
[80] A. Venneri, G. Gorgoglione, C. Toraci, et al., Combining neuropsychological and structural neuroimaging indicators of conversion to Alzheimer's disease in amnestic mild cognitive impairment, Curr. Alzheimer Res. 8 (2011) 789–797, https://doi.org/10.2174/156720511797633160.
[81] J.E. Savage, P.R. Jansen, S. Stringer, et al., Genome-wide association meta-analysis in 269,867 individuals identifies new genetic and functional links to intelligence, Nat. Genet. 50 (2018) 912–919, https://doi.org/10.1038/s41588-018-0152-6.

[82] M. Lam, J.W. Trampush, J. Yu, et al., Large-scale cognitive GWAS meta-analysis reveals tissue-specific neural expression and potential nootropic drug targets, Cell Rep. 21 (2017) 2597–2613, https://doi.org/10.1016/j.celrep.2017.11.028.
[83] D. Baglietto-Vargas, E. Sánchez-Mejias, V. Navarro, et al., Dual roles of Aβ in proliferative processes in an amyloidogenic model of Alzheimer's disease, Sci. Rep. 7 (2017) 10085, https://doi.org/10.1038/s41598-017-10353-7.
[84] H.F. Bradford, M. Docherty, J.-Y. Wu, et al., The immunolysis, isolation, and properties of subpopulations of mammalian brain synaptosomes, Neurochem. Res. 14 (1989) 301–310, https://doi.org/10.1007/BF01000031.
[85] S.R. Robinson, Neuronal expression of glutamine synthetase in Alzheimer's disease indicates a profound impairment of metabolic interactions with astrocytes, Neurochem. Int. 36 (2000) 471–482, https://doi.org/10.1016/S0197-0186(99)00150-3.
[86] G.Sh Burbaeva, I.S. Boksha, E.B. Tereshkina, et al., Glutamate and GABA-metabolizing enzymes in post-mortem cerebellum in Alzheimer's disease: phosphate-activated glutaminase and glutamic acid decarboxylase, Cerebellum 13 (2014) 607–615, https://doi.org/10.1007/s12311-014-0573-4.
[87] T. Wu, M. Hallett, The cerebellum in Parkinson's disease, Brain 136 (2013) 696–709, https://doi.org/10.1093/brain/aws360.
[88] L. Solstrand Dahlberg, O. Lungu, J. Doyon, Cerebellar contribution to motor and non-motor functions in Parkinson's disease: a meta-analysis of fMRI findings, Front. Neurol. 11 (2020), https://doi.org/10.3389/fneur.2020.00127.
[89] J.L. Mirdamadi, Cerebellar role in Parkinson's disease, J. Neurophysiol. 116 (2016) 917–919, https://doi.org/10.1152/jn.01132.2015.
[90] W.P. Flavin, L. Bousset, Z.C. Green, et al., Endocytic vesicle rupture is a conserved mechanism of cellular invasion by amyloid proteins, Acta Neuropathol. 134 (2017) 629–653, https://doi.org/10.1007/s00401-017-1722-x.
[91] J. Shorter, The mammalian disaggregase machinery: Hsp110 synergizes with Hsp70 and Hsp40 to catalyze protein disaggregation and reactivation in a cell-free system, PLoS One 6 (2011), https://doi.org/10.1371/journal.pone.0026319.
[92] N. Yamagishi, M. Yokota, K. Yasuda, et al., Characterization of stress sensitivity and chaperone activity of Hsp105 in mammalian cells, Biochem. Biophys. Res. Commun. 409 (2011) 90–95, https://doi.org/10.1016/j.bbrc.2011.04.114.
[93] H. Rampelt, J. Kirstein-Miles, N.B. Nillegoda, et al., Metazoan Hsp70 machines use Hsp110 to power protein disaggregation, EMBO J. 31 (2012) 4221–4235, https://doi.org/10.1038/emboj.2012.264.
[94] B. Eroglu, D. Moskophidis, N.F. Mivechi, Loss of Hsp110 leads to age-dependent tau hyperphosphorylation and early accumulation of insoluble amyloid β, Mol. Cell Biol. 30 (2010) 4626–4643, https://doi.org/10.1128/mcb.01493-09.
[95] R.U.H. Mattoo, S.K. Sharma, S. Priya, et al., Hsp110 is a bona fide chaperone using ATP to unfold stable misfolded polypeptides and reciprocally collaborate with Hsp70 to solubilize protein aggregates, J. Biol. Chem. 288 (2013) 21399–21411, https://doi.org/10.1074/jbc.M113.479253.
[96] Y. Mao, Q. Kong, R. Li, et al., Heat shock protein A12A encodes a novel prosurvival pathway during ischaemic stroke, Biochim. Biophys. Acta (BBA) Mol. Basis Dis. 1864 (2018) 1862–1872, https://doi.org/10.1016/j.bbadis.2018.03.006.
[97] P. Madsen, T.J. Isaksen, P. Siupka, et al., HSPA12A targets the cytoplasmic domain and affects the trafficking of the amyloid precursor protein receptor SorLA, Sci. Rep. 9 (2019), https://doi.org/10.1038/s41598-018-37336-6.
[98] Q. Ding, W.R. Markesbery, Q. Chen, et al., Ribosome dysfunction is an early event in Alzheimer's disease, J. Neurosci. 25 (2005) 9171–9175, https://doi.org/10.1523/JNEUROSCI.3040-05.2005.
[99] K. Hernández-Ortega, P. Garcia-Esparcia, L. Gil, et al., Altered machinery of protein synthesis in Alzheimer's: from the nucleolus to the ribosome, Brain Pathol. 26 (2016) 593–605, https://doi.org/10.1111/bpa.12335.
[100] A. García-Osta, M. Cuadrado-Tejedor, C. García-Barroso, et al., Phosphodiesterases as therapeutic targets for Alzheimer's disease, ACS Chem. Neurosci. 3 (2012) 832–844, https://doi.org/10.1021/cn3000907.
[101] U.N. Chowdhury, M.B. Islam, S. Ahmad, M.A. Moni, Systems biology and bioinformatics approach to identify gene signatures, pathways and therapeutic targets of Alzheimer's disease, Inf. Med. Unlocked 21 (2020), https://doi.org/10.1016/j.imu.2020.100439.
[102] M.R. Rahman, T. Islam, B. Turanli, et al., Network-based approach to identify molecular signatures and therapeutic agents in Alzheimer's disease, Comput. Biol. Chem. 78 (2019) 431–439, https://doi.org/10.1016/j.compbiolchem.2018.12.011.
[103] Md.S. Uddin, A. al Mamun, Md.T. Kabir, et al., Multi-target drug candidates for multifactorial Alzheimer's disease: AChE and NMDAR as molecular targets, Mol. Neurobiol. 58 (2021) 281–303, https://doi.org/10.1007/s12035-020-02116-9.
[104] M. Tanvir Kabir, M. Sahab Uddin, A. al Mamun, et al., Combination drug therapy for the management of alzheimer's disease, Int. J. Mol. Sci. 21 (2020).